REPORT DOCUMENTATION PAGE

Form Approved OMB NO. 0704-0188

1. REPORT DATE (DD-MM-YYYY)	2. REPORT TYPE	3. DATES COVERED (From - To)
	New Reprint	-

4. TITLE AND SUBTITLE
Microstructural formations and phase transformation pathways in hot isostatically pressed tantalum carbides

5a. CONTRACT NUMBER
W911NF-08-1-0300

5b. GRANT NUMBER

5c. PROGRAM ELEMENT NUMBER
611102

6. AUTHORS
Robert A. Morris, Billie Wang, Lawrence E. Matson, Gregory B. Thompson

5d. PROJECT NUMBER

5e. TASK NUMBER

5f. WORK UNIT NUMBER

7. PERFORMING ORGANIZATION NAMES AND ADDRESSES
University of Alabama - Tuscaloosa
Sponsored Programs
The University of Alabama
Tuscaloosa, AL 35487 -0104

8. PERFORMING ORGANIZATION REPORT NUMBER

9. SPONSORING/MONITORING AGENCY NAME(S) AND ADDRESS(ES)
U.S. Army Research Office
P.O. Box 12211
Research Triangle Park, NC 27709-2211

10. SPONSOR/MONITOR'S ACRONYM(S)
ARO

11. SPONSOR/MONITOR'S REPORT NUMBER(S)
54397-MS.11

12. DISTRIBUTION AVAILIBILITY STATEMENT
Approved for public release; distribution is unlimited.

13. SUPPLEMENTARY NOTES
The views, opinions and/or findings contained in this report are those of the author(s) and should not contrued as an official Department of the Army position, policy or decision, unless so designated by other documentation.

14. ABSTRACT
A series of XTa:(1 □ X)C (0.5 < X < 1) compositions have been fabricated by hot isostatic pressing (HIP) of Ta and TaC powder blends. Depending upon the targeted stoichiometry, single- or multiple-phase microstructures formed. The single-phase microstructures of both TaC and Ta2C had equiaxed grain morphologies. The multiphase microstructures had either equiaxed TaC grains with a crisscross pattern of Ta4C3 laths or acicular grain morphologies with rafts of TaC, Ta4C3 and Ta2C laths running parallel to the major axis of the grains. The effect

15. SUBJECT TERMS
Ceramics; Carbides; Transmission electron microscopy (TEM); Electron backscattering diffraction (EBSD); Precipitation

16. SECURITY CLASSIFICATION OF:			17. LIMITATION OF ABSTRACT	15. NUMBER OF PAGES	19a. NAME OF RESPONSIBLE PERSON
a. REPORT	b. ABSTRACT	c. THIS PAGE			Gregory Thompson
UU	UU	UU	UU		19b. TELEPHONE NUMBER 205-348-1589

Report Title

Microstructural formations and phase transformation pathways in hot isostatically pressed tantalum carbides

ABSTRACT

A series of XTa:(1 □ X)C (0.5 < X < 1) compositions have been fabricated by hot isostatic pressing (HIP) of Ta and TaC powder blends. Depending upon the targeted stoichiometry, single- or multiple-phase microstructures formed. The single-phase microstructures of both TaC and Ta2C had equiaxed grain morphologies. The multiphase microstructures had either equiaxed TaC grains with a crisscross pattern of Ta4C3 laths or acicular grain morphologies with rafts of TaC, Ta4C3 and Ta2C laths running parallel to the major axis of the grains. The effect of phase transformations on the microstructure of these specimens is discussed and compared to those microstructures seen in a reaction diffusion couple formed between Ta and TaC powders processed under the same HIP conditions. This couple revealed the depletion of carbon from the TaC phase and its reaction with the tantalum metal to form the various Ta-rich carbide phases. The precipitation sequence was found to be paramount in controlling the grain morphology. A close-packed plane and direction orientation relationship was seen between all the phases. The crisscross pattern of Ta4C3 precipitation in TaC was a consequence of TaC's multiple variant {111} orientations and had little or no effect on the grain morphology. In contrast, the single variant close-packed plane {0001} in Ta2C resulted in the parallel alignment of the precipitated phases within its grain and an anisotropic growth direction that facilitated the acicular grain morphology.

REPORT DOCUMENTATION PAGE (SF298)
(Continuation Sheet)

Continuation for Block 13

ARO Report Number 54397.11-MS
Microstructural formations and phase transforma ...

Block 13: Supplementary Note

Approved for public release; distribution is unlimited.

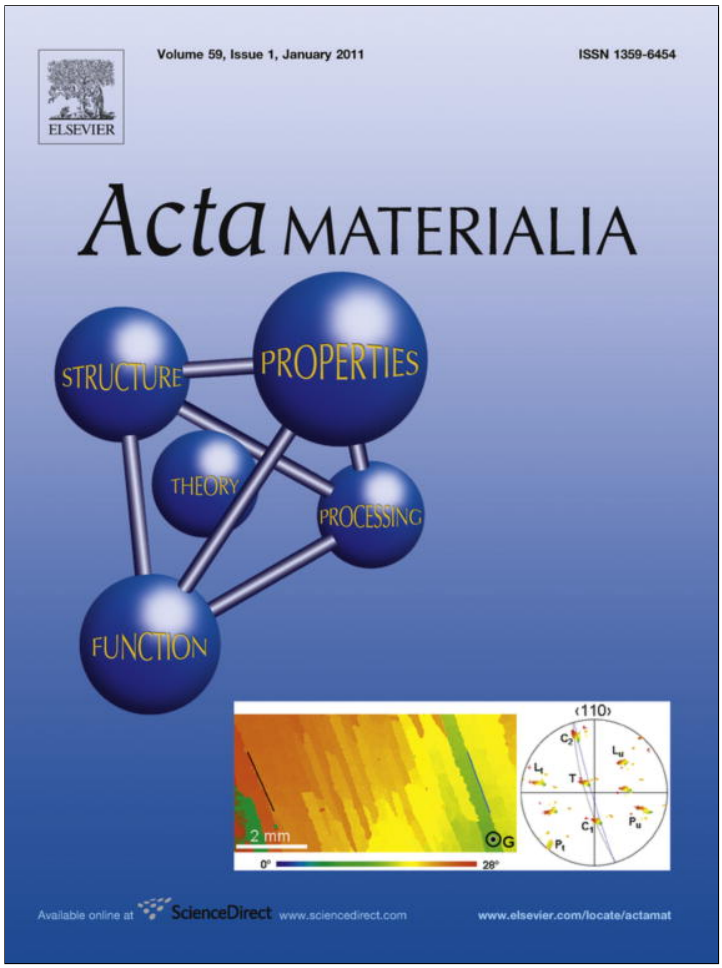

(This is a sample cover image for this issue. The actual cover is not yet available at this time.)

Available online at www.sciencedirect.com

SciVerse ScienceDirect

Acta Materialia 60 (2012) 139–148

Acta MATERIALIA

www.elsevier.com/locate/actamat

Microstructural formations and phase transformation pathways in hot isostatically pressed tantalum carbides

Robert A. Morris [a], Billie Wang [a], Lawrence E. Matson [b], Gregory B. Thompson [a,*]

[a] The University of Alabama, Department of Metallurgical & Materials Engineering, 301, 7th Avenue, 116 Houser Building, Tuscaloosa, AL 35487, USA
[b] Materials and Manufacturing Directorate, AFRL/RXLN Building 655, 2230 Tenth St., Wright- Patterson AFB, OH 45433-7817, USA

Received 21 April 2011; received in revised form 9 September 2011; accepted 21 September 2011

Abstract

A series of XTa:$(1-X)$C ($0.5 < X < 1$) compositions have been fabricated by hot isostatic pressing (HIP) of Ta and TaC powder blends. Depending upon the targeted stoichiometry, single- or multiple-phase microstructures formed. The single-phase microstructures of both TaC and Ta_2C had equiaxed grain morphologies. The multiphase microstructures had either equiaxed TaC grains with a crisscross pattern of Ta_4C_3 laths or acicular grain morphologies with rafts of TaC, Ta_4C_3 and Ta_2C laths running parallel to the major axis of the grains. The effect of phase transformations on the microstructure of these specimens is discussed and compared to those microstructures seen in a reaction diffusion couple formed between Ta and TaC powders processed under the same HIP conditions. This couple revealed the depletion of carbon from the TaC phase and its reaction with the tantalum metal to form the various Ta-rich carbide phases. The precipitation sequence was found to be paramount in controlling the grain morphology. A close-packed plane and direction orientation relationship was seen between all the phases. The crisscross pattern of Ta_4C_3 precipitation in TaC was a consequence of TaC's multiple variant {1 1 1} orientations and had little or no effect on the grain morphology. In contrast, the single variant close-packed plane {0 0 0 1} in Ta_2C resulted in the parallel alignment of the precipitated phases within its grain and an anisotropic growth direction that facilitated the acicular grain morphology.

Keywords: Ceramics; Carbides; Transmission electron microscopy (TEM); Electron backscattering diffraction (EBSD); Precipitation

1. Introduction

Tantalum carbide (TaC) has high hardness and a melting temperature of ~4250 K, which is one of the highest melting points known [1]. Consequently, tantalum carbide has been proposed for use in ultrahigh-temperature load-bearing applications [2–4], such as thermal barrier coatings, machine tools and wear-resistant brake liners. The phase diagram for the tantalum–carbon system [5] is shown in Fig. 1a with corresponding crystal structures shown in Fig. 1b. The ultrahigh melting temperature of TaC and the ability to precipitate similar high-melting-temperature phases offers the potential to engineer its microstructures to meet specific thermal–mechanical property combinations [6].

The TaC phase is a B1 compound (NaCl-based or rock-salt structure), with carbon atoms occupying the octahedral interstitial sites in a tantalum face-centered cubic (fcc) lattice [2,7]. The carbon-deficient Ta_2C phase has a melting temperature of ~3600 K [8,9] and consists of hexagonal metal layers separated by either an α-ordered or β-disordered carbon sublattice. The allotropic phase transformation temperature between α-Ta_2C (CdI_2 antitype structure) and β ($L'3$ structure) is ~2300 K [1,7]. In addition, a ζ-Ta_4C_3 phase, which is rhombohedral with the space group R_3m, can form at ~2775 K [10,11]. The Ta_6C_5 ordered cubic phase (Fig. 1a) represents an ordering of the vacancies on the carbon sublattice, and is thought to form during slow continuous cooling after annealing at

* Corresponding author. Tel.: +1 205 348 1589; fax: +1 205 348 2164.
E-mail address: Gthompson@eng.ua.edu (G.B. Thompson).

1359-6454/$36.00 © 2011 Acta Materialia Inc. Published by Elsevier Ltd. All rights reserved.
doi:10.1016/j.actamat.2011.09.036

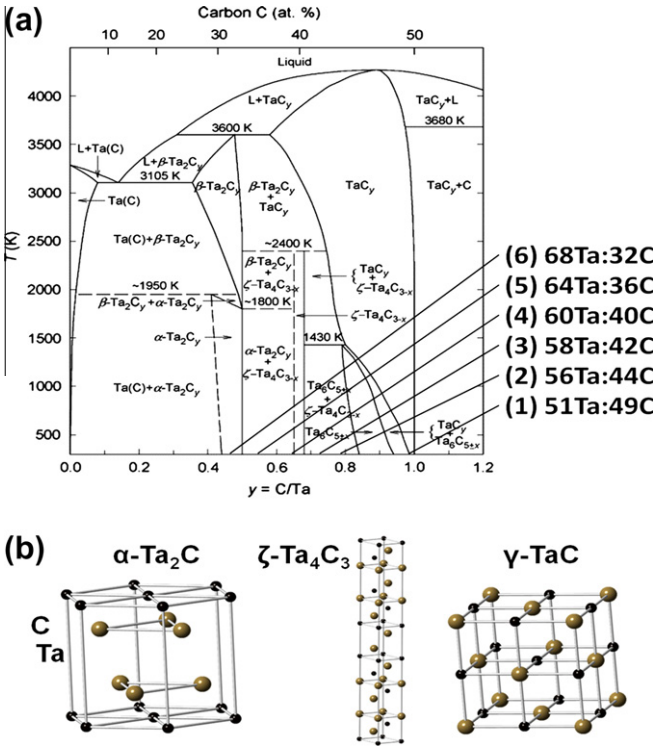

Fig. 1. (a) Ta–C binary phase diagram [9], with the region of the Ta/C content investigated highlighted. Numbers in parentheses identify compositions under investigation and correspond to the samples in Tables 1 and 2. For this work, the Ta_6C_5 regions are considered to be TaC. (b) The three phases of tantalum carbide: hexagonal α-Ta_2C, rhombohedral ζ-Ta_4C_3 and cubic γ-TaC.

elevated temperature [10]. Based on the thermal history of this work, the phase fields designated Ta_6C_5 are considered to be TaC.

One of the significant challenges of developing tantalum carbide alloys and other similar refractory compounds is their high melting points, which limits easy manufacturing to full density and near net shape. Additionally, the carbide systems can decarburize in a vacuum or inert gas atmospheres, which provides a challenge in controlling stoichiometry. This decomposition by incongruent vaporization is seen in the top-down solidification approaches, such as vacuum plasma spray and arc melting [12]. In hot isostatic pressing (HIP), the constituent powders themselves can still volatilize; however, this is minimized within the confines of the HIP can, thus providing process control of the Ta/C molar ratios. Thus a well-blended mixture of powders can reduce or eliminate significant compositional gradients in the final product. Finally, significant plastic flow occurs in the HIP billet, because of the high temperatures and pressures, and this yields near-theoretical densities [13]. In this paper, we report how HIP processing of tantalum carbides with varying compositions affects the precipitation of the different carbide phases and how this affects the resulting microstructure. Previous work has shown critical links between the strength and toughness in tantalum carbides to the volume fraction of phases formed with their corresponding microstructures [6,14]. By understanding the sequence of precipitation, the overall microstructures can ultimately be engineered. To date, there has been little work elucidating how these microstructures develop.

2. Experimental procedures

Two sets of specimens were prepared in order to study the precipitation and formation pathways of tantalum carbides. A set of six HIPed specimens of various Ta/C ratios, XTa:$(1-X)$C, where $X = 51$, 56, 58, 60, 64 and 68 at.%, were prepared by mixing powders of Ta and TaC to nominal compositions, as shown in the phase diagram of Fig. 1a and tabulated in Tables 1 and 2. In addition, a reaction diffusion couple specimen was formed by packing TaC powder onto Ta powder and HIPing under the same conditions as the blended specimens. The compositions produced in the couple included those of the individual specimens and was used to help explain the microstructures that formed from the single composition mixtures. The powders were purchased from Cerac, Inc., and their starting size distribution (Fig. 2) was measured from scanning electron microscopy images in conjunction with the Nikon Elements® imaging analysis software package. The grains sizes were measured using the diameters equivalent area circles, and typically encompassed 50–100 grains per specimen. The powders were placed into tantalum HIP cans using an inert-gas glove box and the tantalum cans were then evacuated and welded closed for subsequent HIPing at 200 MPa in an argon atmosphere at 1873 K for 100 min.

Table 1
The far left column contained the targeted atomic weight compositions. Grain size analysis data for the XTa:$(1-X)$C specimens.

Samples/grain size	Mean diameter (μm)	Mean long axis (μm)
(l) 51Ta:49C	2.2 ± 0.7	2.8 ± 0.9
(2) 56Ta:44C	5.2 ± 2.0	7.0 ± 4.0
(3) 53Ta:42C	8.9 ± 3.6	11.9 ± 4.0
(4) 60Ta:40C	9.6 ± 5.0	18.0 ± 11.1
(5) 64Ta:36C	6.1 ± 4.0	11.0 ± 7.7
(6) 68Ta:32C	23.0 ± 8.8	29.0 ± 10.8

Table 2
The far left column contains the targeted atomic weight compositions, the XRD is the estimated volume fraction of the phases determined by the integrated intensity ratio of the peaks from Fig. 3f, and the lever rule is the compositions based on the XRD volume fraction estimations.

Samples/phase	XRD			Lever rule	
	TaC	Ta_4C_3	Ta_2C	Ta	C
(1) 51Ta:49C	100	0	0	51	49
(2) 56Ta:44C	100	0	0	56	44
(3) 58Ta:42C	96	4	0	58	42
(4) 6QTa40C	49	33	17	61	39
(5) 64Ta36C	7	36	57	65	35
(6) 63Ta32C	0	0	100	68	32

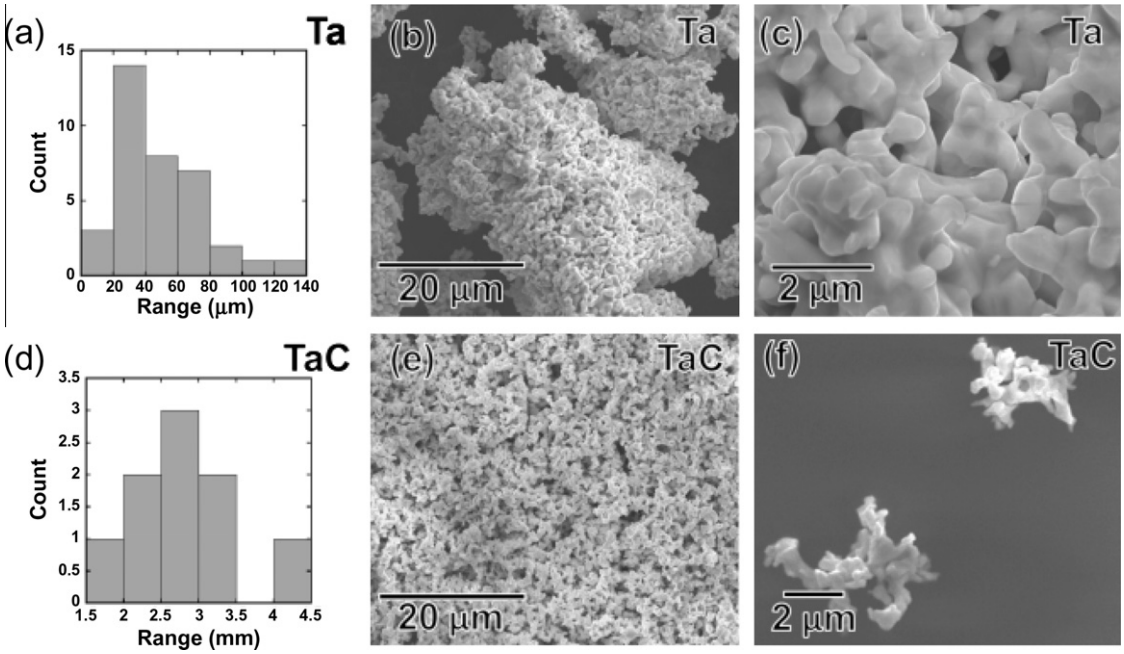

Fig. 2. Grain size data and SEM images from the initial Ta and TaC powders used in the fabrication of the XTa:$(1-X)$C specimens. (a) Distribution histogram of the grain sizes of the Ta powder. (b) SEM image of the Ta powder showing the agglomerated nature of the Ta powders. (c) SEM image of a higher magnification image of the nodular morphology of the Ta powder. (d) Distribution histogram of the grain sizes of the TaC powder. (e) SEM image of the TaC powder. (f) SEM image of two separated TaC powders showing the nodal nature of the powder.

The six XTa:$(1-X)$C post-HIP specimens were removed from their tantalum cans and cut into transverse and longitudinal pieces. These pieces were mounted in cross-section, mechanically ground and polished with a finishing step of 3 micron diamond abrasive paste. These were then placed in a Vibromet® and polished for 24 h in aqueous 0.05 micron silica slurry.

The microstructures were imaged using either secondary electron or ion contrast imaging in an FEI Quanta 3D dual focus ion beam (FIB) scanning electron microscope (SEM) operated at 30 keV. Electron backscatter diffraction patterns, used for phase identification, were collected using the EDAX-TSL platform with a Hikari camera attached to the FEI Quanta 3D microscope. The specimens were tilted 70° towards the detector and scanned at 100 frames per second at an electron beam setting of 30 keV and 5.0 nA.

X-ray diffraction was used for phase identification and volume fraction determination using a Bruker Discovery D8 General Area Diffraction Detector System with Cu K_α radiation at 45 keV and 40 mA at the source. The TaC, Ta_2C and ζ-Ta_4C_3 phases were identified using data from Wyckoff [15], Lissner and Schleid [8] and Gusev et al. [10], respectively. The phase content of the specimens are tabulated in Table 2. They were estimated using the integrated intensity of the theoretically most intense peak for each phase and applying the direct comparison method [16]. The specific peaks used for this analysis were the $\{1\,1\,1\}$ TaC [15], $\{1\,0\,\bar{1}\,7\}$ Ta_4C_3 [8] and $\{1\,0\,\bar{1}\,\bar{1}\}$ Ta_2C reflections [10]. The volume fractions of each phase determined by X-ray diffraction (XRD) were coupled with the phase diagram using the lever rule and were in good agreement with the intended overall composition of each specimen.

For the diffusion couple analysis, energy-dispersive spectroscopy (EDS) was used to determine the approximate Ta and C composition across the reaction interface. The EDS data were collected on an EDAX Apollo XV silicon drift detector at an electron beam setting of 10 keV and 3.3 nA. A 51Ta:49C (TaC) specimen was used as the calibration standard. By reducing the accelerating voltage, the interaction volume for X-ray emission is condensed and potential absorption of C X-rays by Ta was reduced. Good agreement between the EDS measurement and the standard was found at the 10 keV setting.

Transmission electron microscopy (TEM) and scanning transmission electron microscopy (STEM) was performed using an FEI F20 Tecnai microscope operated at 200 keV. Correlated bright- and dark-field imaging and selected area electron diffraction (SAED) were used for phase and microstructure characterization. Complimentary atomic, or Z-, contrast imaging, using a high-angle annular dark field (HAADF) detector, was done in a STEM mode. The HAADF collects scattered electrons that are relatively insensitive to crystallographically dependent (Bragg) scattering; therefore, the contrast observed is chemically dependent, with higher atomic number elements being brighter [17]. TEM specimens were prepared using both the traditional (dimpling and ion milling) method and the FIB milling techniques [18,19]. The FIB milling was conducted on a FEI Quanta 3D dual beam FIB and allowed for site-specific TEM foil extraction.

3. Results

3.1. Characterization of the initial powders

The Ta powders exhibited a large variation in particle size, as shown in the distribution histogram in Fig. 2a. The powders were composed of agglomerated Ta particulates (Fig. 2b), and had an average agglomerate size of 48 ± 25 μm and a log normal distribution. Fig. 2c shows the nodular morphology of the Ta powders. The TaC powder size was considerably smaller, with an average agglomerate size of 2.7 ± 0.7 μm and a normal size distribution (Fig. 2d). Though the nodular morphologies of the TaC and Ta powders were similar (Fig. 2c and f), the TaC powders were qualitatively less agglomerated than the Ta powders (Fig. 2b and f).

3.2. SEM, EDS and XRD characterization of the XTa:(1 − X)C compositions

The six XTa:$(1-X)$C specimens were processed to span the range from single-phase TaC to single-phase Ta_2C, with their multiphase microstructures in between. The desired compositions (nominal), determined by the starting TaC/Ta ratios, were in close agreement to the post-processed HIP compositions determined by the XRD volume fraction-lever rule as well as the EDS analysis. This confirms that minimal carbon loss occurred during the canned HIP processing. Grain size analysis was performed on the SEM micrographs and the results are shown in Table 1. Along with mean grain size, the average maximum Feret size was also measured. The maximum Feret diameter represents the longest dimension of the grain [20] and is used to quantify acicular grain morphologies.

The 51Ta:49C and 56Ta:44C specimens were found to be single-phase TaC, as shown by the XRD phase identification in Fig. 3a. Both compositions had an equiaxed grain microstructure (Fig. 3b; only the 56Ta:44C specimen is shown). These two single-phase compositions confirmed the wide-ranging non-stoichiometry in the TaC phase, as indicated by the phase diagram of Fig. 1a. No Ta_6C_5 phase was found; its absence is attributed to its slow kinetics [10]. As noted previously, the Ta_6C_5 phase region was considered to be TaC.

While the XRD for both 51Ta:49C and 56Ta:44C specimens indicates single-phase TaC, a clear XRD peak shift occurred between the specimens (Fig. 3a). This XRD shift is in the direction of a smaller d-spacing, which would correspond to a sub-stoichiometric TaC (carbon deficient) specimen with a smaller lattice parameter. The 51Ta:49C specimen was found to have a statistically similar grain size (2.2 ± 0.7 μm; Table 1) to that of the starting TaC powder (2.7 ± 0.7 μm; Fig. 2d), suggesting that there was minimal grain coarsening post-sintering during the HIP process. The mean sizes are within a standard error of each other.

The 58Ta:42C specimen had a composition which lies within the two-phase field of TaC and Ta_4C_3 (Fig. 1). XRD of the 58Ta:42C specimen showed that the majority phase was TaC, with minor intensity reflections for Ta_4C_3. The phase content for this specimen, as determined by

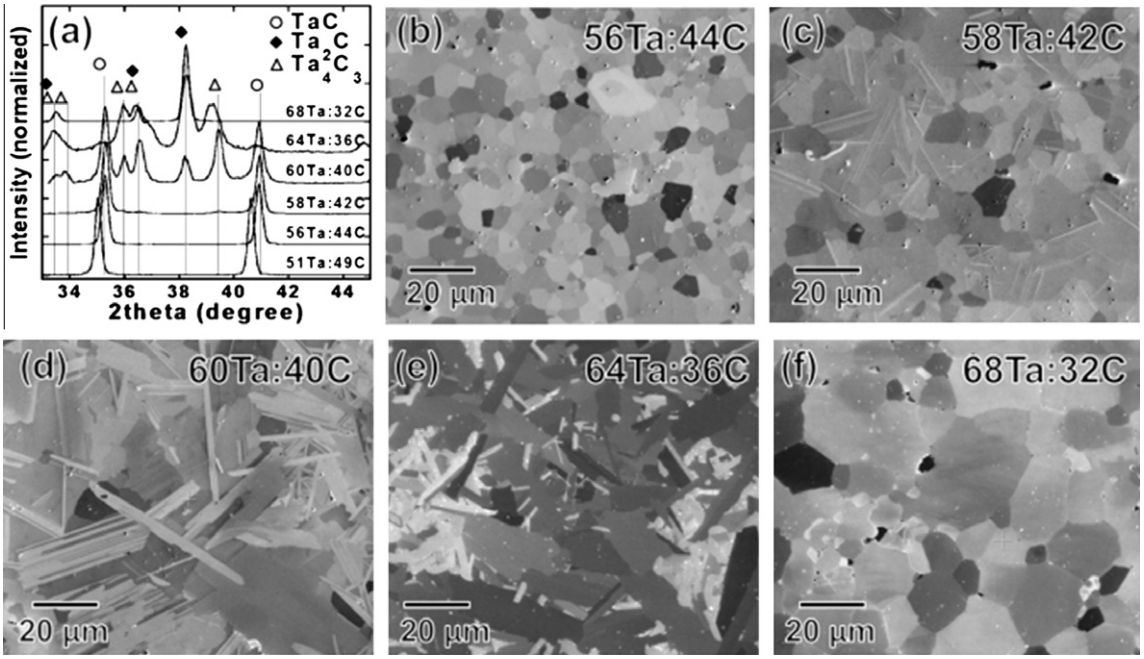

Fig. 3. (a) XRD data of the XTa:$(1-X)$C specimens showing the different phases present depending on composition. Note the variation in TaC peak angle between the 51Ta:49C and 56Ta:44C specimen which indicated a change in carbon content. (b) Ion contrast image using the FIB of the 56Ta:44C specimen showing an equiaxed single-phase TaC microstructure. (c) 58Ta:42C specimen showing precipitated secondary phase laths in multiple directions encased within an equiaxed TaC grain microstructure. (d) 60Ta:40C specimen showing an acicular microstructure with large amounts of secondary phase laths. (e) 64Ta:36C specimen showing an acicular microstructure. (f) 68Ta:32C specimen showing an equiaxed single-phase Ta_2C grain microstructure.

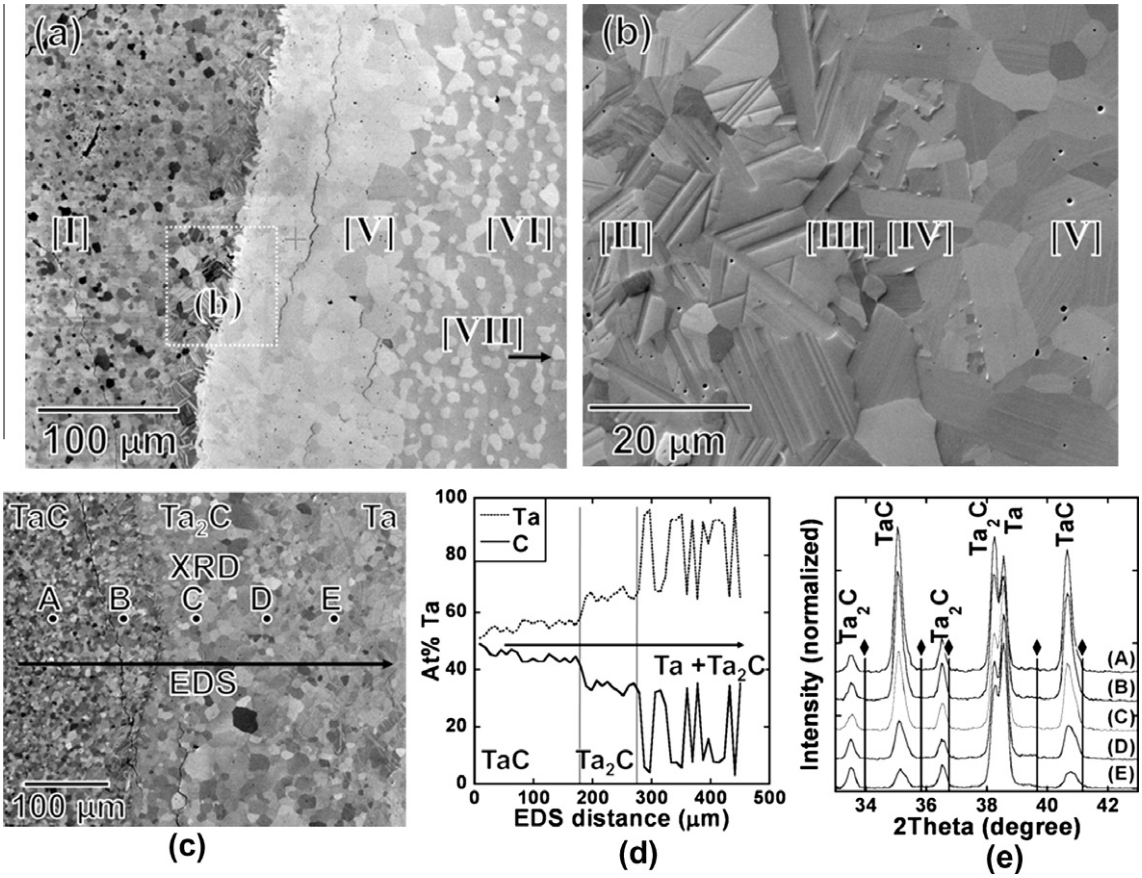

Fig. 4. (a) SEM image of the diffusion couple showing the single-phase TaC region, labeled as [I], through the reaction interface, and finally to the mixture of Ta_2C and Ta grains labeled as [VI]. The equiaxed Ta grains location, labeled region [VII], is not shown, but an arrow points in the direction of its location in the specimen. (b) Higher magnification image of the region of the reaction interface in (a), dotted box, showing the different microstructures along the interface labeled [II]–[V]. (c) SEM image of the diffusion couple showing approximate position for the EDS and XRD line scan data collection spots. (d) EDS line profile showing the different compositions through the different phases of the diffusion couple. (e) XRD data for the line scan showing the variation in peak intensity for each phase in the diffusion couple. Interestingly, there were no reflections corresponding to the Ta_4C_3 phase, as indicated by the diamond-shaped markers (♦), but the phase was evident using electron scattering techniques on the same specimen.

XRD, was ~96 vol.% TaC and 4 vol.% Ta_4C_3. The specimen had an equiaxed grain shape similar to that of the 51Ta:49C and 56Ta:44C specimens, but the SEM micrograph in Fig. 3c clearly revealed multidirectional or crisscross patterns of Ta_4C_3 phase laths. Previous work has revealed that the Ta_4C_3 precipitates on the TaC's {1 1 1} family of close-packed planes [20,21]. Additionally, the grain size increased to 8.9 ± 3.6 μm, indicating an increasing grain size with increasing Ta powder additions in the blend.

The 60Ta:40C specimen exhibited grains that were no longer equiaxed but were acicular in grain morphology (Fig. 3d). The XRD spectra (Fig. 3a) confirmed the increase in Ta_4C_3 and Ta_2C phase content, with the volume fractions of these phases being 49 vol.% TaC, 34 vol.% Ta_4C_3 and 17 vol.% Ta_2C. Unlike the 58Ta:42C specimen, where the laths were crisscrossed in the grain, in this specimen, rafts of parallel laths formed along the major axis of the acicular grain. This increase in lath density and acicular grain morphology has a marked influence on the strength and toughness behavior in tantalum carbides, as previously reported [14]. The mean grain size diameter was found to be 9.6 ± 5.0 μm and, notably, the maximum Feret length was found to be over twice the grain size, with a mean value of 18.0 ± 11.1 μm.

With further depletion in the carbon content, the XRD spectra for the 64Ta:36C specimen showed a continual decrease in the TaC phase content and increased amounts of the Ta_4C_3 and Ta_2C phases. The phase amounts were determined to be 7 vol.% TaC, 36 vol.% Ta_4C_3 and 57 vol.% Ta_2C. As with the 60Ta:40C specimen, the 64Ta:36C specimen exhibited an acicular grain structure (Fig. 3e), with a maximum Feret length of 11.0 ± 7.7 μm.

The 68Ta:32C composition specimen places it in the single-phase field of Ta_2C according to the phase diagram (Fig. 1a). The XRD spectra (Fig. 3a) confirmed that this was the only phase present. Similar to the single-phase TaC, this specimen exhibited an equiaxed grain microstructure (Fig. 3f). A comparison of the single-phase TaC and Ta_2C mean grain diameters, 2.2 ± 0.7 vs. 23 ± 8.8 μm, listed in Table 1, shows a large difference in the grain sizes. As noted previously, the grain sizes for each of the

specimens, listed in Table 2, shows a general increasing trend of grain size with increasing Ta metal content in the initial powder compacts.

3.3. Ta–TaC reaction couple experiment

A reaction couple was fabricated using TaC powder placed adjacent to Ta powder and then processed using the same HIP procedure given above. This resembles the actual HIP process mechanisms that would occur in the single composition specimens fabricated. Using stacked powders and not dense solids allows for bulk diffusion, as well as allowing some surface diffusion over the compacted powders to occur. The clear compositional gradient produced allows the effect of the tantalum–carbon interaction to be highlighted. Seven specific and different microstructural regions that correspond to different carbon compositions in the couple are shown in Fig. 4a and b. Starting on the TaC side of the couple and progressing towards the metallic Ta side, these regions are as follows:

[I] Equiaxed single-phase TaC
[II] Equiaxed TaC grains with lath structures (both single and multiple variants)
[III] Small equiaxed Ta_2C grains
[IV] Acicular Ta_2C grains with aligned stacking faults or laths
[V] Large equiaxed single-phase Ta_2C
[VI] A mixture of equiaxed Ta_2C and Ta grains
[VII] Equiaxed Ta grains

EDS and XRD lines scans were performed on the couple to characterize the different regions. The EDS line scan, shown by the dark arrow in Fig. 4c, shows the relative

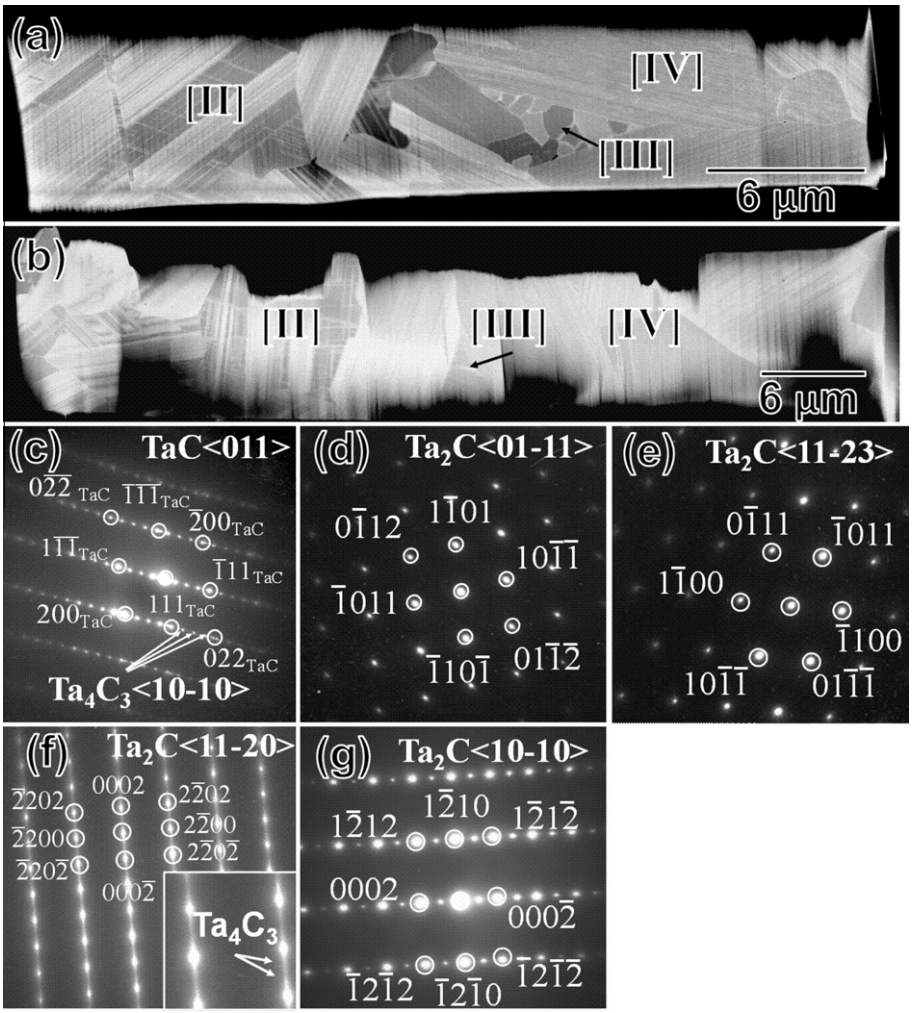

Fig. 5. (a and b) STEM-HAADF images of the reaction interface which showed the secondary phase laths that form within the grains. Both foils were prepared by FIB-based milling extraction [17] at the interface of the diffusion couple. (c) SAED of TaC grain with Ta_4C_3 laths within region [II]. (d) SAED of region [C] indexed as Ta_2C from zone axis $\langle 01\bar{1}1\rangle$. (e) SAED of region [III] indexed as Ta_2C from zone axis $\langle 11\bar{2}3\rangle$. (f) SAED of region [IV] of a Ta_2C grain with the precipitation of Ta_4C_3 from the Ta_2C zone axis $\langle 11\bar{2}0\rangle$. The inset image is a magnified image of the separation in the spots consistent with the Ta_2C and Ta_4C_3 phase identification. The streaking is a result of either rel-rod effects and/or faulting because of the fine, parallel layering of these phases with respect to each other seen in region [IV] in (a) and (b). (g) SAED of region [IV] of a Ta_2C grain with the precipitation of Ta_4C_3 from another Ta_2C zone axis prospective, $\langle 10\bar{1}0\rangle$.

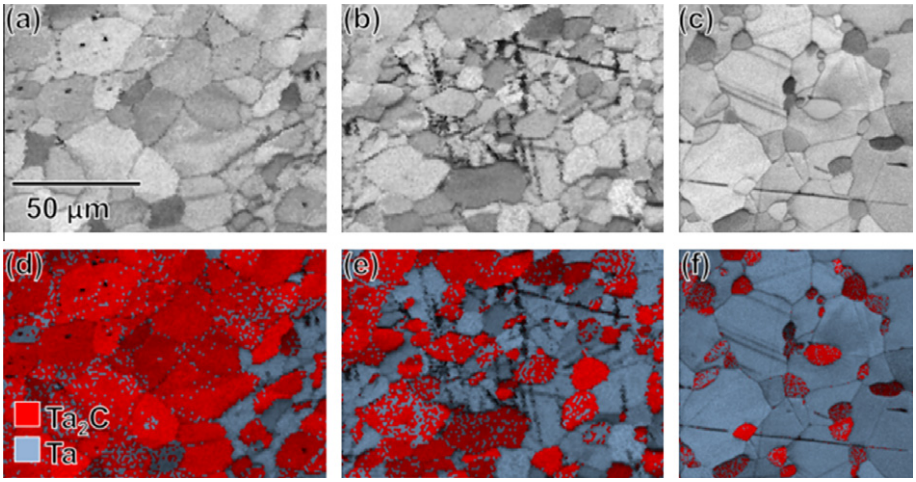

Fig. 6. EBSD image quality maps with corresponding phase maps from regions [VI]. (a and d) Ta_2C rich-side showing Ta_2C larger grains with small Ta grains. (b and e) Mixture of equisized Ta_2C and Ta grains. (c and f) Ta rich-side showing larger Ta grains with Ta_2C grains forming at the grain boundaries.

microstructural location with respect to how carbon content fluctuated across the couple (Fig. 4d). The EDS line profile showed a steady decrease in the carbon content, starting from approximately 50Ta:50C (TaC) and decreasing to 56Ta:44C (sub-stoichiometric TaC). At the 56Ta:44C composition, a significant slope change occurred until a steady-state composition of 66Ta:33C (Ta_2C) was reached. According to the phase diagram (Fig. 1a), this region is where TaC/Ta_4C_3 and Ta_4C_3/Ta_2C should form. Further profiling resulted in an oscillatory carbon signal that varied between 66Ta:33C and 90Ta:10C, which corresponded to grains of either Ta_2C or Ta respectively. Since the electron generated X-ray emission interaction volume is larger than the single Ta phase features or grains, and Ta has little solubility for carbon at 1870 K (Fig. 1a), the detected carbon for the 90Ta:10C is considered to be from surrounding grains.

The XRD line scan (Fig. 4e) was performed over ~400 μm at a spot spacing of 80 μm per step to determine the phase content across the couple. The approximate XRD positions are marked in Fig. 4c. The XRD spectra confirmed TaC, Ta_2C and Ta were present. This suggests that either the Ta_4C_3 phase was not present or it was below the detection limit at each probe location. The XRD spot probe was larger than the grains at the interface. Hence this method was not able to clearly separate specific phases and identify them to their specific spatial locations, but clear trends in the relative rise and fall in phase peak intensities is evident in Fig. 4e. Regardless, the XRD and EDS line profile positions showed relatively good agreement between composition and phase content. To remedy the issue of phase position to specific grain location, TEM (Fig. 5) and EBSD (Fig. 6) phase mapping were conducted.

The microstructure in region [II] of Fig. 4b revealed mostly equiaxed grains. This reaction zone on the TaC side of the couple [II] was approximately 35 μm in width. These grains contained crisscrossed patterns of laths. TEM SAED analysis revealed that these laths were the Ta_4C_3 phase (Fig. 5a–c).

The microstructure in the diffusion couple interface (region [III] in Figs. 4b and 5a) contained very small equaixed grains of the Ta_2C phase, as identified by TEM SAED (Fig. 5d and e). Adjacent to the small equiaxed Ta_2C grains in region [III] is a much larger acicular primary Ta_2C grain structure, in region [IV] (Fig. 5a). These acicular Ta_2C grains contained thin laths, clearly shown by the thin contrast bands in Fig. 5a and b. The grain structure of region [IV], like region [III], was only a few grains thick. TEM SAED analysis in Fig. 5f and g revealed that these very thin laths were Ta_4C_3 encased in Ta_2C acicular grains. The streaking in the diffraction pattern is a result of either rel-rod effects and/or faulting.

Upon approaching the Ta side of the diffusion couple (region [V] in Figs. 4b and 6a), the acicular shape of the Ta_2C grains changed into an equiaxed shape, with no precipitation or faulting. Moving further toward the Ta side of the couple, denoted as region [VI] (Fig. 4a), the equiaxed Ta_2C grains become intermixed with the metallic Ta phase (Fig. 6). Fig. 6 shows three distinct morphological regions in region [VI] from left to right. Fig. 6a, closest to region [V] in Fig. 4a, contains a majority of larger Ta_2C grains with smaller metallic Ta grains. Fig. 6b shows a mixture of equivalent sized Ta_2C and Ta grains. Fig. 6c, closest to region [VII] in Fig. 4a, shows a majority of smaller Ta_2C grains nucleating at the grain boundaries of the larger Ta grains. Fig. 6d–f shows the EBSD phase identification for these different sub-regions.

The average equivalent grain diameters for the different phases in these three sub-regions are tabulated in Table 3.

Table 3
Grain size data for Fig. 6. Data shows similar grain sizes of each of the major phase, *i.e.* Ta_2C grain sizes in the Ta_2C rich-side and Ta grain sizes in Ta rich-side, along with similar grain sizes for the Ta and Ta_2C grains within the middle region in Fig. 7b and e.

Diameter (μm)	(1) Ta_2C side	(2) Middle	(3) Ta side
Ta	9 ± 4.1	11 ± 3.5	17 ± 6.9
Ta_2C	15 ± 5.5	10 ± 4.7	6 ± 2.0

The changes in grain size of each of the Ta_2C and Ta phases are similar, i.e. the major phase size is ~16 μm while the minor phase size is ~7 μm. At the end of the couple (region [VII] in Fig. 4a) were equiaxed metallic Ta grains.

4. Discussion

From the results presented above, small changes in carbon content in tantalum carbides can result in significant changes in grain morphology. For example, the 58Ta:42C has equiaxed TaC grains with Ta_4C_3 secondary phases precipitated on the four variants of the {1 1 1} planes, while 60Ta:40C has acicular grains formed with Ta_4C_3 secondary phases that precipitated parallel to each other and aligned along the major axis of the grain. Complicating these issues is that these phases formed through a reaction of constituent powders.

In general, the specimens which are predominantly equiaxed TaC-phase materials (51Ta:49C, 56Ta:44C, and 58Ta:42C) had smaller grain sizes, between 2 and 9 μm, compared to either the major axis length of the acicular grains (60Ta:40C and 64Ta:36C), 11-18 μm, or the equiaxed Ta_2C materials (68Ta:32C), 23 μm. For single-phase TaC, this can be easily understood by considering the starting powder diameters. The TaC starting powders had a mean size of 2.7 ± 0.7 μm. The mean grain size of the 51Ta:49C sample was 2.2 ± 0.7 μm, suggesting that the powders only sintered together. While the 51Ta:49C sample's grains appear smaller, they are not statistically significantly smaller than the powders, and are within a standard error of each other. In addition, the powders in Fig. 2b–e have a nodular morphology, which may get compacted into a smaller volume during HIPing. The other two equiaxed TaC specimens, 56Ta:44C (sub-stoichiometric TaC) and 58Ta:42C (sub-stoichiometric TaC with some multivariant precipitation of Ta_4C_3), had an increase in the TaC grain size, from 5.2 to 8.9 μm, respectively. This increase is attributed to both thermodynamic curvature growth [12] and the fact that the fine TaC powders were mixed with much larger Ta powders and then reacted.

For the specimens with predominately equiaxed grains, an increase in the proportion of Ta is correlated with an increased grain size. The specimen with the most Ta, 68Ta:32C, Fig. 3f, had the largest average grain size of 23 μm, similar to the initial Ta powder sizes (Fig. 2a). This trend is also observed in the reaction couple experiment with the exception of the interface region [III] of Fig. 5a and b, where the precipitation of very fine equiaxed Ta_2C grain structures occurred. In addition, as the amount of Ta powder increased, a larger standard deviation in grain size occurred (Table 1). While this can be attributed to the variation in Ta powder size for the 68Ta:32C, the intermediate specimens (48Ta:42C, 60Ta:40C and 64Ta:36C) formed from reactions of very differently sized starting powders. Thus, this powder size discrepancy, coupled with the how well these powders are blended, could account for the resulting larger range of final grain sizes seen in these compositions. In general, there appears to be a trend of the final grain size of the processed specimens tracking with the starting constituent powder sizes.

For each composition, the phases presented in the binary phase diagram (Fig. 1a) formed during the HIP process. The Ta_6C_5 phase was not expected because of the rapid cooling in the heat treatment [10]. It is clear that some of these specimens were not yet at equilibrium conditions because all three phases (TaC, Ta_4C_3 and Ta_2C) were still present in two-phase fields (Fig. 1a). For example, specimen 64Ta:36C, which lies in the two-phase region of Ta_2C and Ta_4C_3 according to the phase diagram, still contained about 7 vol.% TaC, according to XRD analysis. Additionally, in all the specimens where Ta_4C_3 formed, it only precipitated out as very fine laths or rafts of laths which never seemed to agglomerate or coarsen (see Figs. 3 and 5).

In the single-phase TaC (51Ta:49C and 56Ta:44C) and Ta_2C (68Ta:32C) alloys, the microstructures were equiaxed. This would be expected since no other phases are present; hence, no interfacial energy contributions were available to drive a particular morphology. Rather, the system forms grains that maximize volume while minimizing surface area. For the specimens that have multiple phases, two distinct morphologies are present: (i) equiaxed grains that encase secondary phases in multiple directions and (ii) acicular grains which have secondary phases parallel to the major axis of the grain.

Equiaxed grains that encase a multidirectional secondary phase (case (i)) are observed in 58Ta:42C and in region [II] of the reaction couple for Figs. 4 and 5. The matrix phase is sub-stoichiometric TaC and the secondary phase is Ta_4C_3. The lath-like structure is attributed to the shearing mechanism, proposed by Rowcliffe [21], on the {1 1 1} planes of TaC. Rowcliffe [21] reported that both the Ta_2C and Ta_4C_3 phases precipitate out of the TaC matrix through a stacking fault mechanism with orientation relationships of $\{1\,1\,1\}_{TaC}//\{0\,0\,0\,1\}_{Ta4C3}//\{0\,0\,0\,1\}_{Ta2C}$; $\langle 1\,1\,0\rangle_{TaC}//\langle 1\,0\,\bar{1}\,0\rangle_{Ta4C3}//\langle 1\,0\,\bar{1}\,0\rangle_{Ta2C}$. This was confirmed by the SAED pattern in Fig. 5c) from region [II] in the reaction couple. Each of these phases has a parallel close-packed plane and close-packed direction orientation relationship with TaC. B1 TaC is a rock-salt structure which has fcc symmetry. If a Shockley partial dislocation of 1/6 $\langle 2\,1\,1\rangle$ passed on every other {1 1 1} fcc plane, the fcc symmetry would convert to the hexagonal close-packed (hcp) structure [21]. To achieve the correct chemistry, every fourth TaC {1 1 1} carbon plane needs to be depleted to form Ta_4C_3 and every other TaC {1 1 1} carbon plane needs to be depleted to form Ta_2C. The removal of these carbon atoms from these particular {1 1 1} planes would generate the required local stacking fault, similar to a Frank loop [22], that would yield the necessary crystal structure. The sequential loss of these carbon atoms drives the chemistry and symmetry changes that form the lath-like structures on these planes. Since TaC has four variants in the {1 1 1} family, this would explain the Ta_4C_3

precipitation in multiple directions, i.e. precipitating on the different {1 1 1} planes. This was confirmed by our reaction couple experiment in region [II] in Fig. 5a and b.

Case (ii) has all the secondary phases precipitated parallel to and along the major axis of the acicular grain, as seen in 60Ta:40C, 64Ta:36C and region [IV] in the couple in Figs. 4 and 5. First, consider the Ta-rich side of the reaction diffusion couple and work towards the TaC phase. As carbon depletes out of the TaC, it diffuses towards the Ta metal powder. The phase diagram in Fig. 1a reveals little or no carbon solubility in tantalum at 1870 K. Consequently, the carbon and tantalum must react and nucleate the first available phase, which is Ta_2C. This is confirmed by Fig. 6c and f, which showed small, equiaxed Ta_2C grains, e.g. initial nucleation sites, on the grain boundaries of the larger Ta grains. Thus the Ta grain boundaries act as fast-track diffusion pathways for carbon and heterogeneous nucleation sites for Ta_2C precipitation. As the Ta_2C grains grow, they consumed the Ta grains around them, resulting in a reduction in the elemental Ta grain size (Fig. 6a). Rodriguez [23] reported that the diffusion rate of carbon in tantalum metal is three orders of magnitude higher than that in TaC and Ta_2C. This difference in diffusion rates allows the carbon to quickly leach out of the TaC and react with the constituent tantalum powder. The diffusion couple effectively shows the process of transformation of Ta into Ta_2C because of the carbon gradient.

As the Ta_2C grains continue to consume more carbon, the precipitation of Ta_4C_3 will occur according to the phase diagram in Fig. 1a. Unlike TaC's fcc-like symmetry, which has multiple close-packed {1 1 1} planes for precipitation of Ta_4C_3 laths, the Ta_2C phase has only one variant of close-packed planes, the {0 0 0 1}, because of its hcp-like symmetry. Thus, for these grains, the Ta_4C_3 only precipitates on one set of planes per grain and the laths run parallel to each other within the grain. The SAED pattern (Fig. 5f and g) from region [IV] in the couple revealed the Ta_2C and Ta_4C_3 phases; both the microstructure and the phase content of region [IV] were similar to the 64Ta:36C specimen. A clear chemical modulation between these phases of region [IV] is seen in Fig. 5a and b by the variation in bright and dark contrast from the HAADF-imaged micrographs. Collectively, these specimens are in good agreement with the phase equilibrium shown in the phase diagram of Fig. 1a. The high aspect ratio of the acicular grains suggests an orientation dependent or anisotropic growth rate, with the fastest growth parallel to the close-packed planes. This leads to a grain conversion into an acicular microstructure, whose major axis is parallel to the close-packed planes (region [IV] in Fig. 5a). These elongated grains are clearly apparent at the interface where carbon content is the highest, and allow the conversion and precipitation process to occur in the initially equiaxed Ta_2C grains. Specimens 60Ta:40C and 64Ta:36C exhibited similar grain morphologies and contained the largest volume fractions of Ta_2C and Ta_4C_3. Further from this reaction couple interface, the equiaxed single-phase Ta_2C grains are preserved. For the single-phase Ta_2C (68Ta:32C) specimen, the reaction of carbon from the initial TaC powders was complete because no elemental Ta was observed in the XRD spectra of Fig. 3a. Additionally, no secondary phases were precipitated in the 68Ta:32C specimen that could alter the grain morphology, so it remained equiaxed.

Lastly, at the interface of the reaction couple, a series of very fine equiaxed grains, region [III] in Fig. 5a and b was indexed as the Ta_2C phase. This is surprising, considering the phase diagram in Fig. 1a. Based on the reaction profile, one would expect this region to be Ta_4C_3. Clearly, the different zone axis diffraction patterns (Fig. 5d and e) show these grains to be Ta_2C. Though carbon would be the fastest diffusing species in the system, and would explain the precipitation and conversion of phases far from the reaction interface, the initial tantalum metal at the interface would also diffuse, though over a much shorter distance, and react with TaC. These small Ta_2C grains at the interface are suspected to have formed as the tantalum reacted with the carbon from the TaC powders to yield Ta_2C. This would be similar to the previous discussion of the initial nucleation and grain formation observed with the smaller Ta grains on the boundaries of the larger Ta_2C grains or smaller Ta_2C grains at the boundaries of the larger Ta grains (Fig. 6). Since the couple is not at thermodynamic equilibrium, the Ta_2C grains have remained.

5. Conclusions

A series of XTa:$(1-X)$C specimens, where $X = 51$, 56, 58, 60, 64 and 68 at.%, were HIP processed from TaC and Ta powder mixtures to span the range from TaC, TaC + Ta_4C_3, Ta_2C + Ta_4C_3 and Ta_2C phase fields. For the single-phase compositions, the microstructure was equiaxed, with the TaC grains being smaller than Ta_2C. The grain size difference was influenced by the initial powder sizes. For composition between ~40 and ~44 at.% C (two-phase regions in Fig. 1a), the microstructure consisted of equiaxed TaC grains encasing fine laths of Ta_4C_3. For compositions between ~34 and ~40 at.% C, a two-phase mixture existed, which contained acicular grains with parallel laths of Ta_4C_3 and Ta_2C. The acicular grain's major axes were parallel to the close-packed planes.

Using a TaC/Ta powder reaction couple, it was observed that carbon is depleted from the TaC phase and precipitated Ta_4C_3 laths on the multiple variant, close-packed {1 1 1} planes of TaC. This resulted in a crisscross pattern morphology seen in region [II] of the couple and in specimen 58Ta:42C. This is in contrast to the parallel lath morphologies observed when Ta_4C_3 precipitates in the hcp-like Ta_2C matrix, where only one close-packed plane {0 0 0 1} is available. Here an acicular grain morphology developed where the laths are parallel along the major axis of the grain, as seen in region [IV] of the couple and in the 60Ta:40C and 64Ta:36C specimens.

Collectively, these results indicate that small variations in carbon content can have a dramatic effect on microstructure morphology and phase content. The sequence of precipitation of the secondary phase from the initial matrix phase, either TaC or Ta_2C, controls the overall grain shape because of the preferred orientation relationship that develops between Ta_4C_3 with either TaC or Ta_2C.

Acknowledgements

This research was supported by the Army Research Office under Grant W911NF-08-1-0300. The authors gratefully thank Dr. Stephan DiPietro of Exothermics, Inc. for the fabricated HIP specimens.

References

[1] Storms EK. The refractory carbides. New York: Academic Press; 1967.
[2] Wang CR, Yang JM, Hoffman W. Mater Chem Phys 2002;74(3):272–81.
[3] Upadhyay K, Yang JM, Hoffman WP. Am Ceram Soc Bull 1997;76(12):51–6.
[4] Balani K, Gonzalez G, Agarwal A, Hickman R, O'Dell JS. J Am Ceram Soc 2006;89(4):1419–25.
[5] Santoro G, Probst HB. Adv X-Ray Anal 1963;7:126–35.
[6] Rowcliffe DJ, Hollox GE. J Mater Sci 1971;6:1261–9.
[7] Barabash OM, Koval YN. A handbook on the structure and properties of metals and alloys. Kiev: Naukova Dumka; 1986.
[8] Lissner F, Schleid T. Z Kristallogr NCS 2001;216(6):329.
[9] Bowman AL. Phys Chem A 1961;65(9):1596–8.
[10] Gusev AI, Kurlov AS, Lipatnikov VN. J Solid State Chem 2007;180:3234–46.
[11] Yvon K, Parthe E. Acta Crystallogr 1970;26:149–53.
[12] German RM. Powder metallurgy and particulate processing. Princeton, NJ: Metal Powder Industries Federation; 2005.
[13] Desmaison-Brut M, Alexandre N, Desmaison J. J Eur Ceram. Soc 1997;17:1326–34.
[14] Hackett K, Verhoef S, Cutler RA, Shetty DK. J Am Ceram Soc 2009;92(10):2404–7.
[15] Wyckoff RWG. Crystal structures. 2nd ed. New York: Interscience Publishers; 1963.
[16] Suryanarayana C, Northon M. X-ray diffraction: a practical approach. New York: Plenum Press; 1998.
[17] Williams DB, Carter CB. Transmission electron microscopy: a textbook for materials science. New York: Springer Science; 1996.
[18] Giannuzzi LA. J Microsc Microanal 2006;12(2):1260–1.
[19] Giannuzzi LA, Geurts R, Ringnalda J. J Microsci Microanal 2005;11(2):828–9.
[20] Kuo CY, Frost JD, Lai JS, Wang LB. Trans Res Rec 1997;1526:98–103.
[21] Rowcliffe DJ. Mater Sci Eng 1975;18:231–8.
[22] Hull D, Bacon DJ. Introduction to dislocations. 4th ed. Woburn, MA: Butterworth-Heinemann; 2001.
[23] Rodriguez PJ. Thesis, The University of New Mexico, Alburquerque, New Mexico; 1996.